Molecular dynamics study of thermal stress and heat propagation in tungsten under thermal shock*

Fu Bao-Qin(付宝勤)†, Lai Wen-Sheng(赖文生), Yuan Yue(袁 悦),
Xu Hai-Yan(徐海燕), Li Chun(李 纯), Jia Yu-Zhen(贾玉振), and Liu Wei(刘 伟)‡

Key Laboratory of Advanced Materials (MOE), School of Materials Science and Engineering, Tsinghua University, Beijing 100084, *China*

(Received 17 January 2013; revised manuscript received 30 May 2013)

Using molecular dynamics (MD) simulation, we study the thermal shock behavior of tungsten (W), which has been used for the plasma facing material (PFM) of tokamaks. The thermo-elastic stress wave, corresponding to the collective displacement of atoms, is analyzed with the Lagrangian atomic stress method, of which the reliability is also analyzed. The stress wave velocity corresponds to the speed of sound in the material, which is not dependent on the thermal shock energy. The peak pressure of a normal stress wave increases with the increase of thermal shock energy. We analyze the temperature evolution of the thermal shock region according to the Fourier transformation. It can be seen that the "obvious" velocity of heat propagation is less than the velocity of the stress wave; further, that the thermo-elastic stress wave may contribute little to the transport of kinetic energy. The heat propagation can be described properly by the heat conduction equation. These results may be useful for understanding the process of the thermal shock of tungsten.

Keywords: molecular dynamics simulation, thermal shock, thermo-elastic stress, heat propagation, tungsten

PACS: 66.70.–f, 66.10.cd, 66.70.Df **DOI:** 10.1088/1674-1056/22/12/126601

1. Introduction

The thermal shock of a solid with a short-pulse high heat flux load gives rise to many material behaviors, such as cracking failure,[1] melting, recrystallization,[2] and ablation,[3,4] which will influence the potential applications of the material under extreme conditions. The plasma facing materials (PFMs) in tokamaks must withstand high thermal fluxes, plasma and neutron fluxes, and high mechanical stresses. Their failures can lead to serious consequences for tokamak working programmes. Therefore, a large amount of effort has been made to perform the high heat load tests on PFMs in recent years.[1,2,5–16] The mechanisms of thermal shock are complex. Tungsten (W) and tungsten-based materials are being considered to be used in the tokamak as PFMs, owing to their low sputtering yield, low tritium retention, no chemical erosion, good thermo-mechanical properties and high thermal conductivity.[1,2,17–19] Currently, W has been designed to be used for the divertor dome and baffle region.[17] During transient events, such as disruptions, edge localized modes (ELMs), and vertical displacement events (VDEs), the divertor armor materials can be exposed to high heat flux loads. Specially, a heat flux of 10 MW/m^2–100 MW/m^2 with a duration ranging from milliseconds to several seconds is predicted to be produced in a VDE.[2] Therefore, in order to understand the mechanisms of heat transport and material failure under such extreme conditions, it is necessary to investigate the thermal shock behavior of tungsten.

In this work, we investigate the thermal shock behavior under an ultrafast heat load, where we focus on the processes of an instantaneous heat load of tungsten thin films. Numerical simulations based on the molecular dynamics (MD) technique play an important role in this field.[3,4,18,20–27] Belonoshko[20] has investigated the Hugoniot equation of state at the transition of argon (Ar) from solid to liquid undertaken by shock wave with a three-dimensional (3D) MD simulation. Upadhyay and Urbassek[4] have studied the fragmentation patterns of ultrathin metal films as a function of the initial energization with MD simulation. Urbassek *et al.*[23] have analyzed the heat transfer from a laser heated metal to an adjacent transparent liquid dielectric with MD simulation. They have found the Kapitza effect at the interface, which was also reported in our early work.[18,26,27] Gu and Urbassek[3] have studied the excitation of stress waves in crystalline Ar over layer films adsorbed on the Pt substrate with MD simulation.

Our work is concerned with MD simulation of thermal stress and heat propagation of tungsten under a sudden heat flux load, which is important for understanding the process of high heat load tests on tungsten. One aim of our simulations is to study the mechanism and process of the thermal stress propagation at the atomic level and its possible effects on material failure. Another aim is to discuss the mechanism and process of the heat propagation combined with many numerical methods.

The rest of this paper is organized as follows. In Sec-

*Project supported by the National Magnetic Confinement Fusion Science Program of China (Grant No. 2013GB109004) and the National Natural Science Foundation of China (Grant Nos. 51071095 and 50971077).

†Corresponding author. E-mail: bqfuthu@163.com

‡Corresponding author. E-mail: liuw@mail.tsinghua.edu.cn

© 2013 Chinese Physical Society and IOP Publishing Ltd

tion 2, we will briefly describe the interatomic potential that we have used. In Section 3, we will explain the simulation method in detail, including the simulation cell, some statistical physics methods, and the calculation of equilibrium unit cell parameters. The results and discussion are presented in Section 4.

2. Interatomic potential of tungsten

Tungsten exists in two major crystalline forms: alpha-W and beta-W. The alpha-W has a body centered cubic structure, belongs to the A2-type crystal structure[28] and is in the most stable form. Therefore, the alpha-W is used for our investigation and the atomic system is described by an empirical N-body potential proposed by Finnis and Sinclair (F-S potential).[29,30] In the F-S potential, the total potential energy of the system is expressed as

$$E = \sum_{j>i} V(r_{ij}) - A\sum_i \sqrt{\sum_{j(\neq i)} \phi(r_{ij})}, \tag{1}$$

where $V(r_{ij})$ is the central pair-potential energy between atom i and atom j; it can be expressed as

$$V(r_{ij}) = \begin{cases} (r_{ij}-c)^2 (c_0 + c_1 r_{ij} + c_2 r_{ij}^2), & r_{ij} \le c, \\ 0, & r_{ij} > c, \end{cases} \tag{2}$$

and $\phi(r_{ij})$ is the charge density of atom i derived from the contribution of the extra-nuclear electron of atom j and it can be expressed as

$$\phi(r_{ij}) = \begin{cases} (r_{ij}-d)^2 + \dfrac{\beta}{d}(r_{ij}-d)^3, & r_{ij} \le d, \\ 0, & r_{ij} > d. \end{cases} \tag{3}$$

The seven parameters A, β, c, c_0, c_1, c_2, and d are free for fitting experimental data or the crystal parameters. For tungsten, they are 18.96373 eV/nm, 0.0, 0.325 nm, 4713.46499 eV/nm^2, -33766.5655 eV/nm^3, 62541.999 eV/nm^4, and 0.4400224 nm, respectively.[29]

3. Simulation method

Through solving the motion equation of the atoms interacting with the F-S potential, MD can simulate the detailed evolution behaviors of all atoms and calculate the physical parameter of the system. We simplify the process of single thermal shock loading from the laser or electrons into such a process that one part of the tungsten thin film is heated and the remaining part is not heated. Therefore, in order to simulate the experimental thermal shock analogously, the schematic representation of the 3D simulation cell is shown in Fig. 1. The crystallographic orientations of the x, y, and z directions are [100], [010], and [001]. The initial configuration for the simulation cell consists of W atoms with $m \times n \times n$ unit cells translated in the x, y, and z directions, respectively, with m being 200 and n varying from 6 to 10 in different simulations. Calculations with various values of n show that $n = 6$ is sufficient to obtain reliable results. In this paper, n is set to be 8.

As shown in Fig. 1, the right region of the simulation cell is called the thermal shock region, which includes 1280 W atoms and is imposed by the heat flux load through scaling the velocities of these atoms in the region at the beginning of the simulation. For the convenience of the discussion and simulation, the remaining atoms are located at the equilibrium position (0 K) at the beginning. The atoms in the left region (five atomic layers, the width is more than the cut-off radius of the F-S potential) are kept fixed at their original positions at all times and periodic boundary conditions are applied in the y and z directions for getting rid of the boundary effects. After the initial thermal shock, the system is allowed to evolve freely. In this work, many cases with various thermal shock energies are simulated, but the main features of the thermal shock process will be described and analyzed particularly in the case of a thermal shock energy of 1.30619×10^9 J/m^3, which means that the initial temperature of the thermal shock region is set to be 1000 K initially.

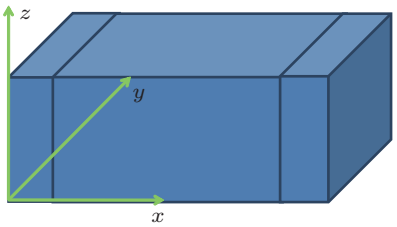


Fig. 1. (color online) Schematic diagram showing the simulated system. The atoms in the left region are kept fixed in the simulation and the right part is thermal shock region.

The simulation cell is divided into several slice layers (s-layer) along the x direction and some thermodynamic parameters of these s-layers will be calculated by a statistical physics method. The temperature can be calculated since the Boltzmann distribution function allows the straightforward derivation of the kinetic energy (E_k) in the following way:

$$E_k = \sum_i^N \frac{1}{2} m_i v_i^2 = \frac{3}{2} N k_B T, \tag{4}$$

where N is the atomic number, m_i the mass of atom i, v_i the atomic velocity, and k_B is the Boltzmann constant. In the MD simulation, the overall or the local atomic stress of systems can be computed by Virial stress definition ($\sigma_{\alpha\beta}$), i.e.,

$$\sigma_{\alpha\beta} = \frac{1}{V}\sum_i \left(-m_i v_{i\alpha} v_{i\beta} + \frac{1}{2}\sum_{j\neq i} (r_{j\alpha} - r_{i\alpha}) f_{ij\beta} \right), \tag{5}$$

where V is the reference volume, α or β denote the x, y or z axis, $v_{i\alpha}$, and $r_{i\alpha}$ are the α-th component of the velocity and the position of atom i and $f_{ij\alpha}$ is the α-th component of the force exerted on atom i by atom j. However, this

kind of atomic stress is the intensity value of the atomic volume, which is entirely different from the finite element method (FEM) which is based on continuum mechanics.[25] In order to correspond to the Cauchy stress, one of the most important quantities in the theoretical framework of continuum mechanics, the fundamental Lagrangian atomic stress[31,32] is used to calculate the atomic stress. The definition is

$$\boldsymbol{n}\boldsymbol{\sigma}_L = \left\langle \frac{1}{A} \sum_{i \in L} \boldsymbol{f}_{i \leftarrow R} \right\rangle, \tag{6}$$

where $\boldsymbol{n}$ is the unit normal vector of the right plane of one s-layer, $\boldsymbol{n}$ is the (1,0,0) in this work and $\boldsymbol{\sigma}_L$ is the stress tensor. Therefore, the left side of formula (6) is equal to (σ_{xx}, σ_{xy}, σ_{xz}), the first one is normal stress, which can also be denoted by σ_x in this paper, and the remaining two are the shear stress. L denotes the reference s-layer, A is the area of the $\boldsymbol{n}$ plane, and $\boldsymbol{f}_{i \leftarrow R}$ is the force on atom I, exerted by the atoms out of the $\boldsymbol{n}$ plane, which can be easily calculated by[32]

$$\boldsymbol{f}_{i \leftarrow R} = \boldsymbol{f}_i - \boldsymbol{f}_{i \in L}, \tag{7}$$

where $\boldsymbol{f}_i$ is the total force acting on atom i and $\boldsymbol{f}_{i \in L}$ is the remaining total force acting on atom i after imaginarily removing the atoms on the right side of the $\boldsymbol{n}$ plane. In the MD simulation, $\boldsymbol{f}_i$ can be calculated in the realistic system and $\boldsymbol{f}_{i \in L}$ can be calculated in the imaginary system only including the atoms in the left hand of the $\boldsymbol{n}$ plane. Since the fundamental Lagrangian atomic stress can be used to obtain the correct Cauchy stress under any circumstance,[32] the Lagrangian atomic stress will be the main stress form to discuss the thermal stress propagation in the remainder of this work.

Before the simulation of thermal shock, the equilibrium unit cell parameter (a) is determined according to the potential energies of the system and the stresses of these s-layers. The atomic internal energies and the stresses of simulation systems with various cell parameters from $a = 0.316495$ nm to 0.316555 nm are calculated. As shown in Fig. 2, the ε–a curve is the same as a parabola and the atomic internal energy (ε) is lowest when a is 0.316520 nm. A linear relationship between σ_x and a is observed and a is also equal to 0.316520 nm when $\sigma_x = 0$ Pa. Therefore, the equilibrium unit cell parameter is 0.316520 nm. Based on the σ_x–a curve, the bulk modulus can be deduced by the slope. The value is 310.5 GPa, which is close to the reference value (310 GPa). This can also prove the reliability of the Lagrangian atomic stress method. The shear stress values are also plotted in Fig. 2. It can be noted that all shear stresses are close to 0 Pa, which is due to the symmetry of the atoms out of the $\boldsymbol{n}$ plane.

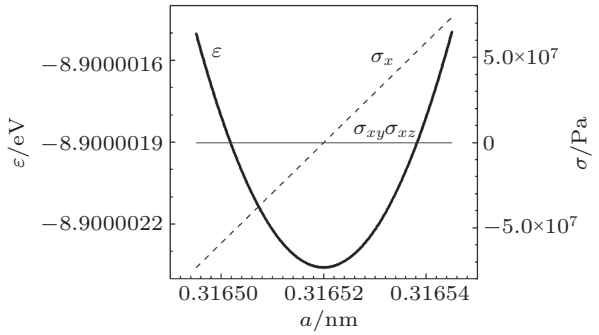


Fig. 2. The thick solid line (parabolic) denotes the atomic internal energy-cell parameter (ε–a) curve. The dash line is the normal stress-cell parameter (σ_x–a) curve. The thin (red) solid line is the shear stress-cell parameter (σ_{xy}–a and σ_{xz}–a) curve.

4. Results and discussion

4.1. Snapshots

Figure 3 shows the snapshots of the left part of the simulation cell (including 142 layers of atoms, about 22.5-nm thick) at various times from 1 picosecond (ps) to 10 ps under thermal shock of 1.30619×10^9 J/m^3. In these snapshots, atoms are colored according to their magnitude of kinetic energy and the red color means that the kinetic energy of the atom is more than 0.005 eV ($T \approx 50$ K). It can be seen that the kinetic energy spreads along the x direction after thermal shock in the hot region due to the heat conduction. At the time of 1 ps (Fig. 3(a)), the kinetic energy focuses on the part near the thermal shock region and the left part is still perfect crystalline ($T = 0$ K). The evolution of the temperature profile will be analyzed in detail in Subsection 4.3. In this case, the vacancies, interstitial W atoms, and adatoms are not seen and all atoms are arranged regularly. However, as shown in Fig. 4,

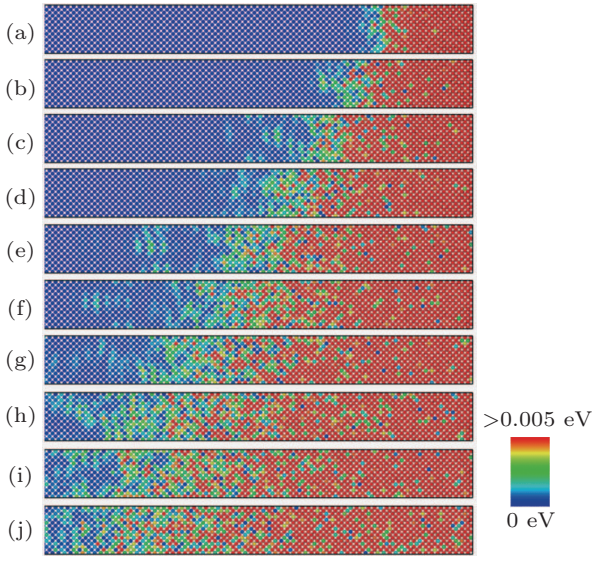


Fig. 3. (color online) The series of snapshots of the right part (142 layers) of the simulation cell at various times ((a): 1 ps, (b): 2 ps, (c): 3 ps, (d): 4 ps, (e): 5 ps, (f): 6 ps, (g): 7 ps, (h): 8 ps, (i): 9 ps, (j): 10 ps) under thermal shock of 1.30619×10^9 J/m^3 at $t = 0$ ps. The color of the tungsten atom denotes the temperature in Kelvin.

with the energy of thermal shock rising from 3.91856×10^{8} J/m^3 to 1.30619×10^{10} J/m^3, some disorder shows up in the thermal shock region and the W-vacuum surface starts to rough and some W atoms are shown on the W surface due to the thermal expansion of the thermal shock region.

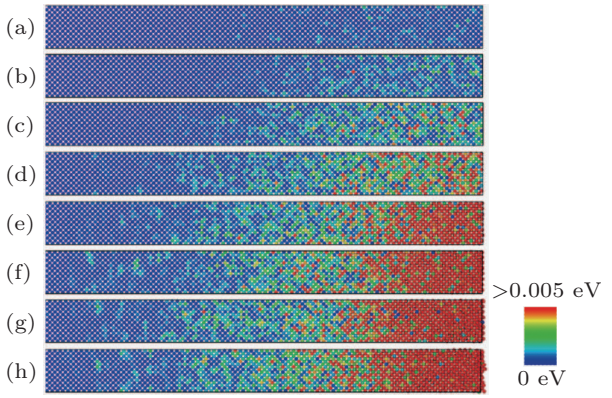


Fig. 4. (color online) The series of snapshots of the right part (164 layers) of the simulation cell at the time of 10 ps under various thermal shock energies ((a): 0.39186, (b): 0.65309, (c): 1.30619, (d): 2.61237, (e): 5.22475, (f): 7.83712, (g): 10.44949, (h): 13.06186) $\times10^{9}$ J/m^3 at $t = 0$ ps. The color of the tungsten atom denotes the temperature in Kelvin.

4.2. Stress

A quite general phenomenon induced by thermal shock is the generation of stress waves. Figure 5 shows the normal stress (σ_x) results obtained with the Lagrangian atomic stress method. It can be seen that normal stress spreads along the x direction after the thermal shock. In our calculation, the normal stress wave has not yet reached the fixed region, which is important that the complications due to wave reflection be ignored. The first main normal stress peak is caused by sudden thermal expansion as the thermal shock is applied.[22] The atoms lying in equilibrium position are first subjected to the force from the right side of the s-layer. Therefore, the atoms in one s-layer shift toward the x negative direction and then toward the x positive direction, as shown in Fig. 6. The average atomic displacement of one s-layer (Δx) can be calculated from the following formula:

$$\Delta x = \sum_i (r_{i1} - r_{i10}), \tag{8}$$

where r_{i1} and r_{i10} are the first component of the actual position and equilibrium position of atom i of one s-layer respectively. So the normal stress of the first main peak is negative, which implies the compressive nature. The compressive region is connected with the tensile region with a series of oscillations. The bipolar nature of the stress wave demonstrates the collective and coherent excitation of oscillations in the tungsten crystal, as explained in Ref. [3]. It should also be noted that the maximum average atomic displacement of one s-layer is about 0.0008 nm ($0.002a$), which is far smaller than the vacancy criterion ($0.3a$).[33] So there is no point defect occurring in the case as shown in Fig. 3.

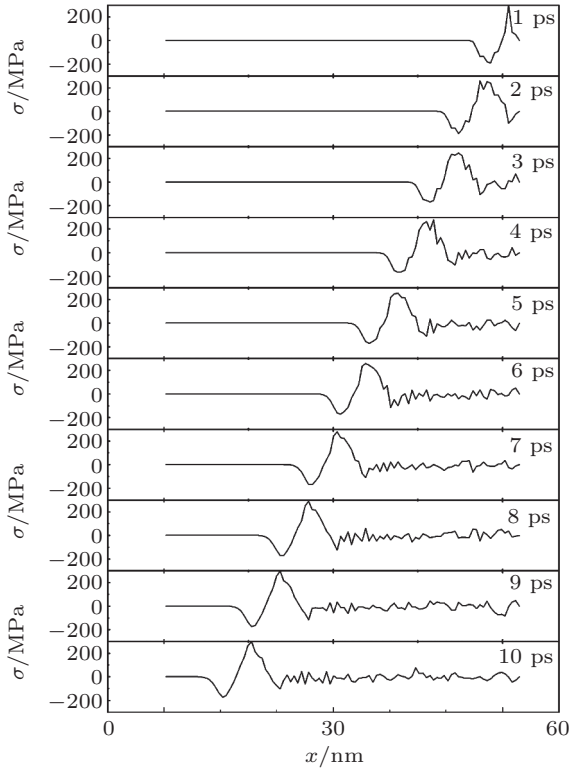


Fig. 5. Evolutions of the normal stress (σ_x) distributions along the x direction (Lagrangian atomic stress method).

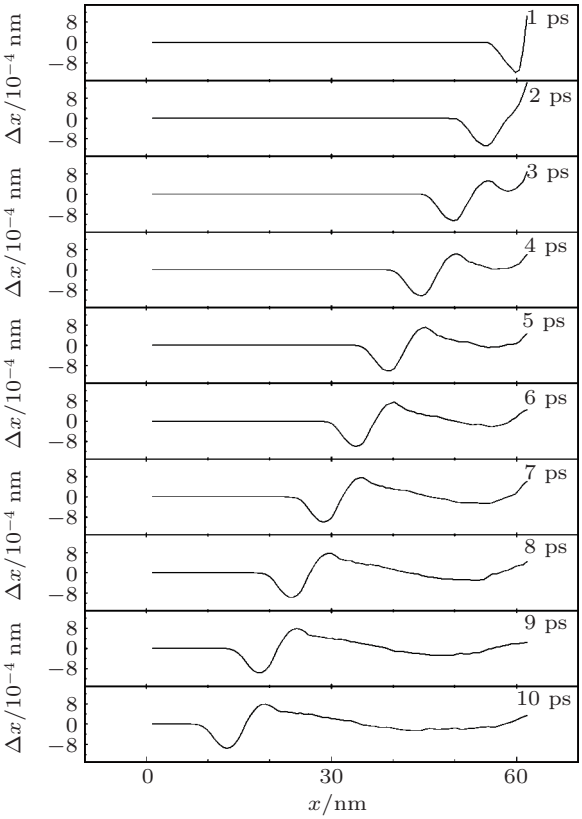


Fig. 6. Evolutions of the average atomic displacement of one s-layer (Δx) distributions along the x direction.

Once the normal stress wave travels away from the thermal shock region, it retains its shape and also its peak value. The peak compressive and tensile pressures are of a similar magnitude. For the case of thermal shock of 3.91856×10^8 J/m^3, the peak pressure is about 292 MPa (tensile pressure peak). The tensile stress generated may lead to the spallation of the material, when it becomes stronger than the yield strength of the material.[3] However, at 77 K in the [100] crystallographic orientation, the proportional limit of the stress–strain curve of tungsten single crystal is 700 MPa,[34] and Roundy *et al.*[35] have reported that the ideal tensile strength of [100] crystallographic orientation was 29.5 GPa. Therefore, the thermal stress may not cause material failure in such a thermal shock energy. However, the peak pressure varies with thermal shock energy. As shown in Fig. 7, we obtain the peak pressures at various thermal shock energies. It can be seen that the peak pressure increases gradually with the increase of thermal shock energy. The relationship between the peak pressure and thermal shock energy is almost linear and the slope is 6.4346×10^{-7}, which is related to the Gruneisen coefficient.[3]

After the normal stress wave of the thermal shock has passed, the stress value returns to a relatively small value fluctuated around 0. For the case of high thermal shock energy, the feature is more obvious. The velocity of the normal stress wave can be determined from Fig. 5 or Fig. 6; it amounts to 5272.8 m/s. This is in good agreement with the longitudinal velocity of sound in the annealed tungsten, which can be deduced from pertinent elastic modulus (B)

$$v = \sqrt{B/\rho}, \tag{9}$$

where ρ is the density of tungsten (19.25388 g/cm^3). So the longitudinal velocity of sound in tungsten is 5220 m/s. For all cases with various thermal shock energies, the calculated normal stress velocities are also obtained, as shown in Table 1. These variations appear to be rather small ($< 1.5\%$), so the normal stress wave velocities are independent of the thermal shock energy.

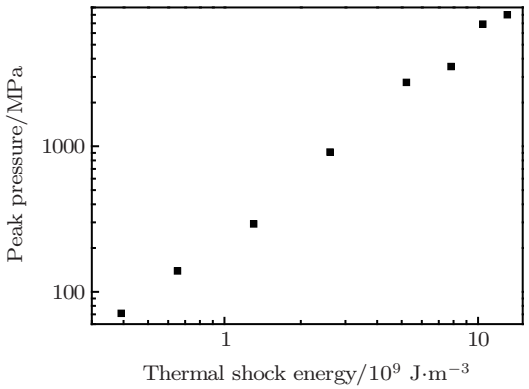


Fig. 7. Peak pressures of normal stress wave increasing with the increase of thermal shock energy.

Table 1. Normal stress wave velocities of various thermal shock energies.

Thermal shock energies/10^9 J·m^{-3}	0.39186	0.65309	1.30619	2.61237	5.22475	7.83712	10.44949	13.06186
Wave velocities/m·s^{-1}	5207.8	5272.8	5272.8	5274.4	5233.3	5222.2	5201.1	5201.1

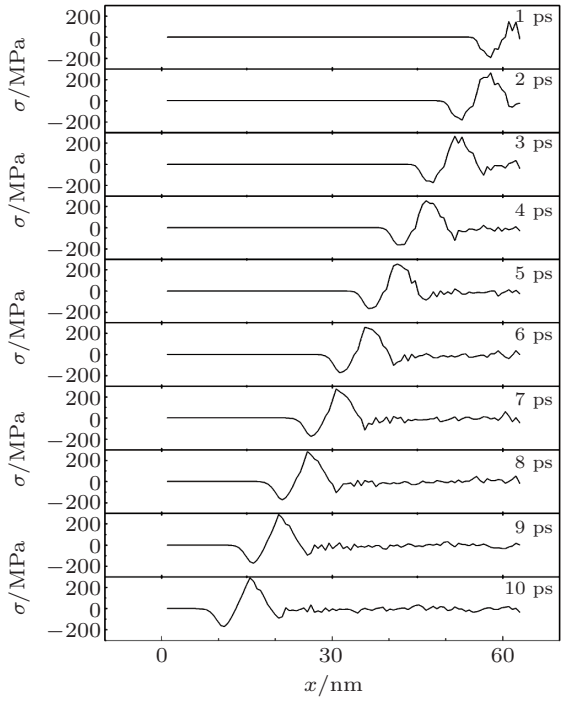


Fig. 8. Evolutions of the Virial normal stress (σ_x) distributions along the x direction.

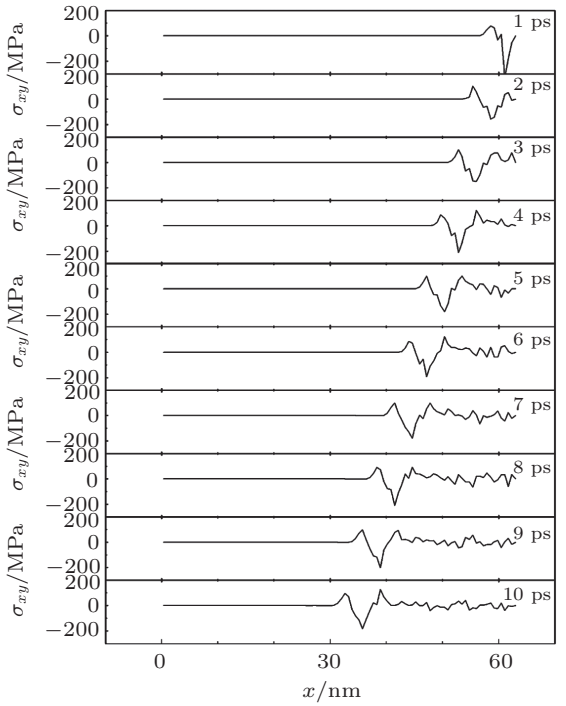


Fig. 9. Evolutions of the shear stress (σ_{xy}) distributions along the x direction (the Lagrangian atomic stress method).

The Virial stress results are also calculated as shown in Fig. 8, which are almost entirely the same as the Lagrangian atomic stress results. It is also proved that the Lagrangian atomic stress method is reliable.

Figure 9 shows the shear stress (σ_{xy}) results obtained with the Lagrangian atomic stress method. Compared with the normal stress curve, the shear stress curve has a most obvious feature, i.e., the velocity of the shear stress wave is less than that of the normal stress wave velocity. The velocity of the shear stress wave is 2877.8 m/s, which is well consistent with the transverse velocity of sound in the annealed tungsten (2890 m/s). Similarly, the shear stress wave velocities are independent of the thermal shock energy, as indicated by the analysis in the cases of the other thermal shock energies.

4.3. Heat propagation

Heat propagation is accomplished through collective movements of discrete atoms in the system. The evolution of the local temperature (i.e., the kinetic energy) of the thermal shock region is shown in Fig. 10. It can be seen that the temperature changes dramatically with a period from 0 ps to 1.5 ps. As explained in Ref. [36], in order to identify the modes and vibrations responsible for heat propagation, the Fourier transform of temperature $T(t)$ is performed by the following expression:

$$F(\nu) = \int_{-\infty}^{+\infty} T(t) \exp(-\mathrm{i}2\pi\nu t)\, \mathrm{d}t. \tag{10}$$

As shown in Fig. 11, there exist two obvious wave peaks in the power spectrum, which may be related to the transverse wave phonons and the longitudinal wave phonons. These modes reflect the dissipative characteristics of the evolution of the temperature (kinetic) in the thermal shock region.[36] It should be pointed out that the Fourier transform curve is smoothed to eliminate noise interference.

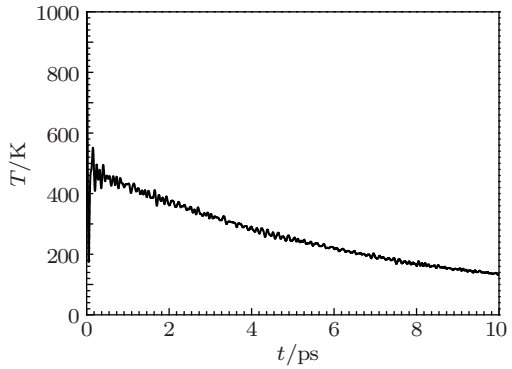


Fig. 10. Evolutions of the local temperature of the thermal shock region.

Figure 12 shows the temperature distributions along the x direction at different times. Compared with these snapshots of various times (Fig. 3), the evolution of the temperature profile is easy to understand. It can be seen that the temperature near the thermal shock region drops gradually and the kinetic energy diffuses toward the x negative direction. The velocity of heat propagation is difficult to determine from Fig. 12 and based on the obvious temperature wave front, the "obvious" velocity of heat propagation can be deduced to be about 2000 m/s, which is far less than the velocity of the stress wave. Thermal energy is transported by phonons that travel randomly in all directions. Therefore, the thermo-elastic stress wave may contribute little to the transport kinetic energy.

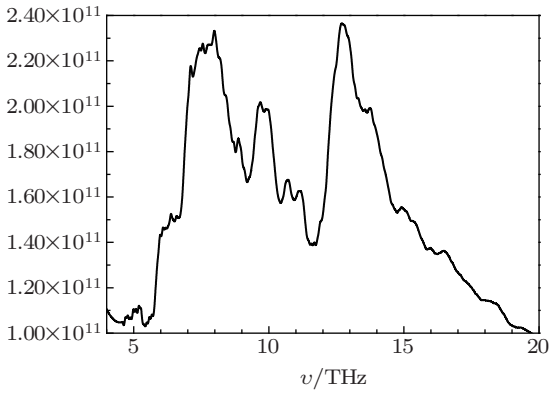


Fig. 11. Fourier transform (power spectrum) of the local temperature of the thermal shock region. The typical frequencies are 8, 9.7 and 12.6 THz.

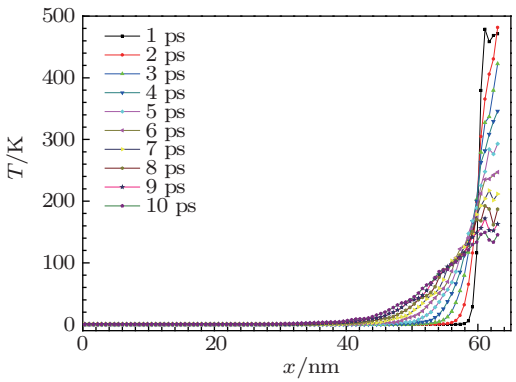


Fig. 12. (color online) Local temperatures of these s-layers along the x direction at various times.

In order to analyze the heat propagation problem, we employ the following continuum approach.[23,37,38] Consider the following 1-d heat conduction problem of a semi-infinite medium. The governing equation for the heat conduction problem without the heat generation term in the medium can be shown as

$$a^2 \frac{\partial^2 T(x,t)}{\partial x^2} = \frac{\partial T(x,t)}{\partial t}, \tag{11}$$

where $a^2 = \kappa/c\rho$ is the thermal diffusivity, κ the thermal conductivity, c the specific heat capacity (the molar heat capacity is 24.27 J/(mol·K)) and ρ the density of the medium. It is assumed that these parameters are constant and independent of the temperature of the medium. Here the initial condition is $T(x,0) = 0$ and two boundary conditions are $T(0,t) = T_0(t)$ and $T(\infty,t)$=0, where $T_0(t)$ denotes the evolution of the local temperature of the thermal shock region ($T(t)$). The above

heat conduction equation can be solved with the Laplace transformation in time and yields

$$T(x,t) = \frac{x}{2a\sqrt{\pi}} \int_0^t \frac{T_0(\tau)}{(t-\tau)^{3/2}} \exp\left(-\frac{x^2}{4a^2(t-\tau)}\right) \mathrm{d}\tau. \quad (12)$$

Therefore, the MD results of the temperature distributions along the x direction can be fitted by the above equation. Further, for the case of 10 ps, the MD results and the fitting results are shown in Fig. 13. It can be concluded that the heat propagation can be described properly by the above equation based on the Laplace transformation. The thermal conductivity can be calculated from the fitting thermal diffusivity to be $\kappa = 16.293$ W/(m·K). The value is close to the lattice thermal conductivity (17.28034 W/(m·K)) at 300 K. It should be noted that the minor mismatch near the surface between the fitting results and MD results may be explained by the surface effect.

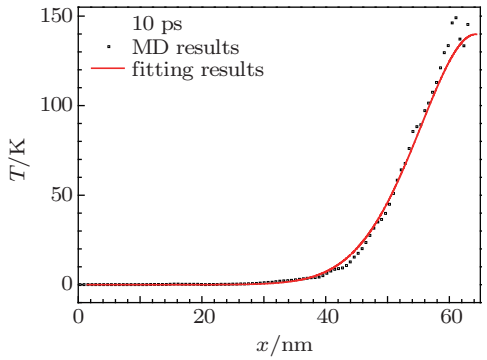


Fig. 13. (color online) Molecular dynamics simulation results of local temperature of these s-layers along the x direction at the time 10 ps; the fitting results are obtained according to the heat conduction equation.

5. Conclusions

In this work, we investigated the thermal shock behavior with a molecular dynamics (MD) simulation, including thermal stress and heat propagation. Firstly, we visually analyzed the process of thermal shock with some snapshots. Then we analyzed the reliability of the Lagrangian atomic stress method through comparing the reference results with the Virial stress results. The thermo-elastic stress wave, corresponding to the collective displacement of atoms in one system, travels with the speed of sound into material. The normal stress wave velocity corresponds to the longitudinal velocity and the shear stress wave velocity corresponds to the transverse velocity, which is independent of the thermal shock energy. The peak pressure of a normal stress wave increases with the increase of thermal shock energy, which may cause material failure in the case of a high heat flux load. In order to identify the modes and vibrations responsible for heat propagation, we calculated the power spectrum of the temperature evolution of the thermal shock region according to the Fourier transformation. It can be analyzed that the "obvious" velocity of the heat propagation is less than the velocity of the stress wave; further, the thermo-elastic stress wave contributes little to the transport of kinetic energy. The heat propagation can be described properly by the heat conduction equation. The MD results are in agreement with the results obtained from a finite element simulation. These results can help understand the process of a high heat load test on tungsten.

References

[1] Hirai T, Pintsuk G, Linke J and Batilliot M 2009 *J. Nucl. Mater.* **390** 751
[2] Yuan Y, Greuner H, Boswirth B, Krieger K, Luo G N, Xu H Y, Fu B Q, Li M and Liu W 2013 *J. Nucl. Mater.* **433** 523
[3] Gu X and Urbassek H M 2006 *J. Phys. D: Appl. Phys.* **39** 4621
[4] Upadhyay A K and Urbassek H M 2006 *Phys. Rev B* **73** 35421
[5] Giniatulin R, Gervash A, Komarov V L, Makhankov A, Mazul I, Litunovsky N and Yablokov N 1998 *Fusion Eng. Des.* **39** 385
[6] Bondarenko G G and Udris Y Y 1998 *Fusion Eng. Des.* **39** 419
[7] Tokunaga K, Yoshida N, Kubota Y, Noda N, Imamura Y, Oku T, Kurumada A, Sogabe T, Kato T and Plochl L 2000 *Fusion Eng. Des.* **49–50** 371
[8] Visca E, Libera S, Orsini A, Riccardi B and Sacchetti M 2000 *Fusion Eng. Des.* **49** 377
[9] Masaki K, Taniguchi M, Miyo Y, Sakurai S, Sato K, Ezato K, Tamai H, Sakasai A, Matsukawa M, Ishida S and Miya N 2002 *Fusion Eng. Des.* **61–62** 171
[10] Liu X, Tamura S, Tokunaga K, Yoshida N, Noda N, Yang L and Xu Z 2004 *J. Nucl. Mater.* **329** 687
[11] Linke J, Escourbiac F, Mazul I V, Nygren R, Rodig M, Schlosser J and Suzuki S 2007 *J. Nucl. Mater.* **367** 1422
[12] Norajitra P, Gervash A, Giniyatulin R, Hirai T, Janeschitz G, Krauss W, Kuznetsov V, Makhankov A, Mazul I, Ovchinnikov I, Reiser J and Widak V 2009 *J. Nucl. Mater.* **386–388** 813
[13] Li H, Chen J L, Li J G and Sun X J 2009 *Fusion Eng. Des.* **84** 1
[14] Greuner H, Boswirth B, Boscary J, Friedrich T, Lavergne C, Linsmeier C, Schlosser J and Wiltner A 2009 *Fusion Eng. Des.* **84** 848
[15] Visca E, Escourbiac F, Libera S, Mancini A, Mazzone G, Merola M and Pizzuto A 2009 *Fusion Eng. Des.* **84** 309
[16] Gavila P, Riccardi B, Constans S, Jouvelot J L, Vastra I B, Missirlian M and Richou M 2011 *Fusion Eng. Des.* **86** 1652
[17] Federici G 2006 *Phys. Scr.* **2006** 1
[18] Fu B Q, Lai W S, Yuan Y, Xu H Y and Liu W 2012 *J. Nucl. Mater.* **427** 268
[19] Li M, Wang J and Hou Q 2012 *J. Nucl. Mater.* **423** 22
[20] Belonoshko A B 1997 *Science* **275** 955
[21] Zhakhovskii V V, Nishihara K, Anisimov S I and Inogamov N A 2000 *JETP Lett.* **71** 167
[22] Ho J R, Twu C J and Hwang C C 2001 *Phys. Rev. B* **64** 14302
[23] Urbassek H M, Gu X and Rethfeld B 2006 *Comp. Mater. Sci.* **38** 51
[24] Zhakhovskii V V and Inogamov N A 2010 *JETP Lett.* **92** 521
[25] Xia R H, Tian X G and Shen Y P 2010 *Acta Mech. Sin.* **26** 599
[26] Fu B, Lai W, Yuan Y, Xu H and Liu W 2013 *Nucl. Instrum. Method B* **303** 4
[27] Fu B Q, Lai W S, Yuan Y, Xu H Y and Liu W 2013 *Nucl. Instrum. Method B* **303** 162
[28] Fu B Q, Liu W and Li Z L 2009 *Appl. Surf. Sci.* **255** 8511
[29] Finnis M W and Sinclair J E 1984 *Philos. Mag. A* **50** 45
[30] Dai X D, Kong Y, Li J H and Liu B X 2006 *J. Phys: Condens. Matter* **18** 4527
[31] Zhou M 2003 *Proc. Roy. Soc. Lond. Ser. A: Math. Phys. Engin. Sci.* **459** 2347
[32] Liu B and Qiu X 2009 *J. Comput. Theor. Nanosci.* **6** 1081
[33] Wang J W, Shang X C and Lü G C 2011 *Adv. Mater. Res.* **179** 513
[34] Beardmore P and Hull D 1965 *J. Less Common Metals* **9** 168
[35] Roundy D, Krenn C R, Cohen M L and Morris J W Jr 2001 *Philos. Mag. A* **81** 1725
[36] Oligschleger C and Schon J C 1999 *Phys. Rev. B* **59** 4125
[37] Stevens R J, Smith A N and Norris P M 2005 *J. Heat Transfer* **127** 315
[38] Stoner R J and Maris H J 1993 *Phys. Rev. B* **48** 16373